# Half width leaky wave antennas

G.M. Zelinski, G.A. Thiele, M.L. Hastriter, M.J. Havrilla and A.J. Terzuoli

**Abstract:** Leaky travelling wave antennas that use the first microstrip higher-order mode are analysed. The antennas investigated here are only half the width of previous leaky wave designs and utilise a structure that inherently suppresses the fundamental mode. Since mode purity is assured, the need for an elaborate feed structure is eliminated. A means for extracting the complex propagation constant of a leaky wave antenna is presented using the finite difference time domain (FDTD) method. Agreement is shown between the resulting propagation constant and another established theoretical method, the transverse resonance method. Representative measured far-field patterns are included, which are consistent with the computed propagation constants. The properties of curving the leaky wave structure are also studied.

## 1 Introduction

Microstrip antennas are attractive because of their light weight, low profile and low cost. These antennas may be grouped into two classes:

1. resonant patch, which is narrowband with a fixed main beam, and
2. nonresonant leaky wave antenna, which typically has a wider bandwidth with a frequency-steerable main beam.

A leaky wave antenna must be excited by a higher-order mode [1], since the fundamental mode of microstrip does not produce fields that decouple from the structure. If the fundamental mode is not allowed to propagate, the next higher-order mode may dominate above its cutoff frequency. Fig.1*a* shows the electric field lines due to the first higher-order mode $EH_1$, as defined by Bagby *et al* [2]. A phase reversal, or null, appears along the centreline that results in oppositely-directed $E$ fields at the edges, allowing the fields to decouple and radiate.

In the late 1970s, Ermert [3, 4] was the first to publish the properties of higher-order microstrip modes. However, his work was incomplete because his longitudinal propagation constant consisted solely of a phase constant $\beta$, but neglected the leakage constant $\alpha$. At about the same time, Menzel [5] published a paper on a microstrip transmission line antenna employing the first higher-order mode. He assumed there was a meaningful leakage constant to allow the structure to radiate, but he did not recognise that he had developed a leaky wave antenna and, thus, built it too short [6, 7]. Oliner [1] further clarified the fact that Menzel had actually built a leaky travelling wave antenna with a complex propagation constant.



doi:10.1049/iet-map:20060011

Paper first received 20th January and in revised form 1st May 2006

G.M. Zelinski is with the Air Force Research Laboratory (AFRL) Wright-Patterson AFB, OH 45433

G.A. Thiele is with the Electrical and Computer Engineering Department, University of Dayton, Dayton OH

M.L. Hastriter, M.J. Havrilla and A.J. Terzuoli are with the Department of Electrical and Computer Engineering, Air Force Institute of Technology, Wright-Patterson AFB, OH 45433

E-mail: gregory.zelinskil@wpafb.af.mil

Since the late 1970s there have been a number of papers on microstrip leaky wave propagation. Leaky wave propagation has been studied in [2], [8–10] and leaky wave antennas in [11–17], although, the potential of these antennas has not been fully explored.

The performance parameters of a travelling wave antenna can be predicted as a function of the wavenumber in the direction of propagation within the structure. Referencing the main beam to endfire ($\theta = 90^\circ$ and $\phi = 0^\circ$), the guided wave phase constant $\beta$ determines the direction of the main beam, and the guided wave attenuation constant $\alpha$ determines the beamwidth of the main beam. Both constants together determine the leaky wave bandwidth. Walter [18] provides an excellent source for analysis of travelling wave antennas.

Determination of the complex propagation constant proved quite difficult for the authors using measurements. While it may be possible to extract a 'ball park' propagation constant from far-field measurements, the accuracy and precision are questionable. Near-field probing techniques show promise but can be time-consuming and laborious [19]. To this end, this work validates its findings by showing agreement between two independent established theoretical methods, the finite difference time domain (FDTD) method and the transverse resonance method.

Fig. 1*b* shows a design enhancement based on Menzel's antenna that incorporates a metal bifurcation down the centerline to block the fundamental mode. Symmetry along this metal wall prompts the application of image theory. One entire side of the antenna is now an image of the other side, making it redundant and not needed. The resulting modified antenna in Fig. 1*c* is half the width of Menzel's antenna. Menzel's original full-width design, which uses seven slots cut from the conductor along the centreline to suppress the fundamental mode, can be seen in Fig. 1*d*. Menzel's antenna requires great effort to develop the appropriate slot structure and feed to reduce the $EH_0$ mode as much as possible.

The use of a shorting wall to reduce the size of microwave 'patch' antennas is well known [20]. However, it is believed that the use of a shorting wall has not previously been applied to microstrip leaky wave antennas to reduce their size. A purpose of this paper is to investigate the reduced size, or half-width (HW), microstrip leaky wave antenna.

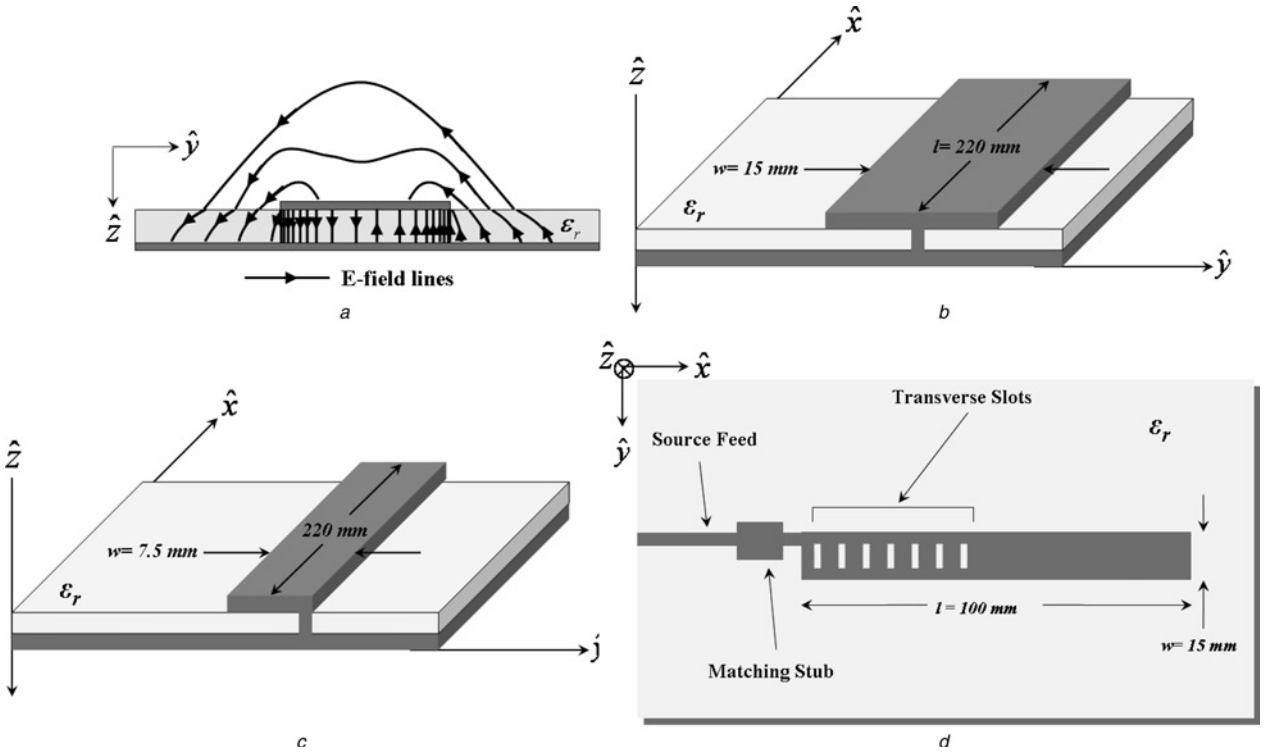


**Fig. 1** *The leaky travelling wave antennas that were analysed*

*a* Electric field pattern associated with the first higher-order mode of microstrip $EH_1$ [2]
*b* Cross-section of the full-width (FW) antenna, which incorporates a metal bifurcation along its entire midline
*c* Cross-section of the half-width (HW) antenna, with a metal bifurcation (wall) attached to its entire right-hand edge
*d* Menzel's original full-width antenna [5], HW and FW antennas use a feed structure similar to the Menzel antenna, although, they do not require a matching stub

Advantages of the half-width (HW) antenna compared to the Menzel antenna are:

(*a*) no need to suppress the $EH_0$ mode;
(*b*) no slot cross-polarised radiation that reduces radiation efficiency;
(*c*) purer guided mode compared to the Menzel configuration, which improves radiation efficiency; and
(*d*) potentially less interaction in an array environment.

## 2 FDTD simulation

### 2.1 Determination of $\alpha$ and $\beta$

The objective of the FDTD simulations was to provide the propagation constant of the vertical component of the electric field $E_z$ inside the substrate between the top conductor and the bottom ground plate. The $E_z$ data was retrieved from a single row of cells stretching the length of the antenna in the $\hat{x}$-direction near the open edge. The logarithm of the normalised magnitude of the $\hat{z}$-directed electric field from these cells created a waveform from which $\alpha$ and $\beta$ were extracted using

$$E_z = \mathrm{e}^{-(\alpha+j\beta)x}$$
$$\ln E_z = -\alpha x - j\beta x \quad (1)$$

As shown in Fig. 2, $\alpha$ is the slope of the peaks of ln $E_z$ (shown as a dotted line) and $\beta$ is found from the separation of nulls using

$$\beta = \frac{2\pi}{\lambda_\beta} \quad (2)$$

Provided the simulation runs long enough to ensure steady state in which the travelling wave distribution has a constant wavelength, only an antenna length of $\lambda_\beta/2$ in the $\hat{x}$-direction is needed for determination of the wavenumber.

### 2.2 The Computational domain

The three antennas of Fig. 1 were investigated for performance. An FDTD algorithm [21] was used employing a 3-D central differencing Yee-cell formulation with a uniaxial perfectly-matched layer (UPML). The UPML was 10-cell-thick, fourth-order polynomial graded and PEC-backed on all six faces. The loss mechanism was normalised to free space to allow layers of unlike materials within the PML.

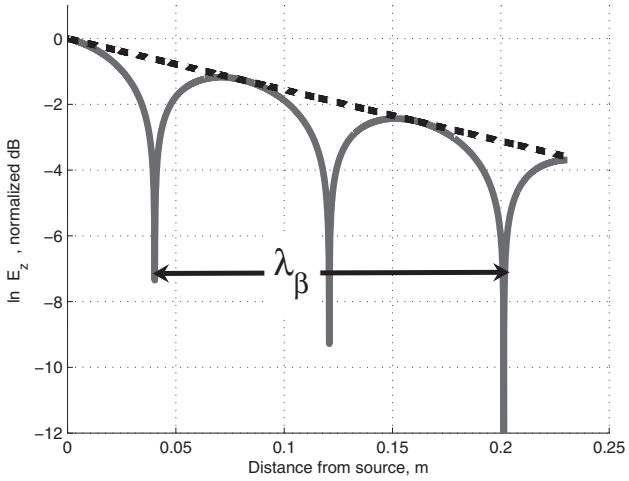


**Fig. 2** *Natural logarithm of the simulation data used to determine the propagation constant in the $\hat{x}$-direction.*

$\alpha$ is the slope of the dashed line and $\lambda_\beta$ is the distance between three successive nulls

The copper conductor was modelled as a zero-thickness perfect electric conductor (PEC) by setting the tangential electric field to zero at the desired cell boundaries. Sheen [22] demonstrated that modelling a microstrip patch antenna in this fashion actually causes the model to perform as if the PEC is extended one-half of a cell further on all open edges due to the FDTD method. This work supports his findings. Care was taken to accurately model the width of the antenna in the $\hat{y}$-direction by reducing the width of the FDTD antenna model by one-half of a cell for the HW antenna and one entire cell for the FW.

The excitation means was a hard source, as defined by Taflove and Hagness [21], and was modelled at the field point closest to the midpoint of the substrate thickness. The source waveform was a constant sinusoid with cubic growth over the first few periods to eliminate the problematic high-frequency components of rapid transitions. Simulations were run for every frequency point of interest. Had computer resources become an issue, a pulse waveform would have been a more elegant solution that would have yielded the data for all frequencies in a single trial.

To isolate the forward travelling wave, the reflections from the free space boundaries at the ends of the substrate needed to be eliminated. This was accomplished by extending the substrate directly into the UPML, and modifying the affected UPML cells to match the substrate. The resulting grid space for the full-width (FW) antenna is seen in Fig. 3. The UPML absorbs all outward propagating waves in the substrate allowing the forward travelling wave to develop exclusively.

For the model of the FW antenna, a $[\mathrm{d}x : \mathrm{d}y : \mathrm{d}z] = [0.4722 : 0.1546 : 0.1574]$ mm grid discretisation was used, which is roughly [3 : 1 : 1], with [Ny, Nz] = [96, 5] cells in the $\hat{y}$-and $\hat{z}$-directions, respectively. Note that, in the $\hat{y}$-direction, the antenna width is $96 \times 0.1546$ mm $\cong$ 14.84 mm, which is approximately one dy reduction from the actual antenna's width of 15 mm. The number of cells in the $\hat{x}$-direction varied with frequency. While it is possible to determine the propagation constant with as little as one-half $\lambda_\beta$, it is easier to gauge steady state from waveform progression with over two $\lambda_\beta$ in length.

Likewise, the HW model also used a [0.4722: 0.1546: 0.1574] mm discretisation with [48, 5] cells in the $\hat{y}$-and $\hat{z}$-directions, respectively. In the $\hat{y}$-direction, the antenna width is $48 \times 0.1546$ mm $\cong$ 7.42 mm, which is approximately one-half dy reduction from the actual antenna's width of 7.5 mm. Again, the number of cells in the $\hat{x}$-direction varied with frequency.

The standard CFL stability condition was used to determine the time-step. Simulation times were as short as 5 min for the highest frequencies up to as long as 8 h for the lowest frequencies.

Convergence was met within 0.1% of the extracted wavenumber for all trials. Resolution within the dielectric exceeded 50 cells per wavelength for all HW and FW trials. The substrate modelled, Rogers Duroid 5870 high-frequency laminate, has a nominal loss tangent of only 0.0012 at 10 GHz. FDTD trials demonstrated that neglecting this loss in the band of interest, 6–8 GHz, affected the extracted propagation constant by no more than 1% and freed nearly 50% of the memory. To further reduce memory demands of the largest simulations, single precision was used resulting in approximately 40% decrease in memory usage. These parameters allowed all simulations to be accurately run on a 2.75 GHz PC with only 1 GB of RAM.

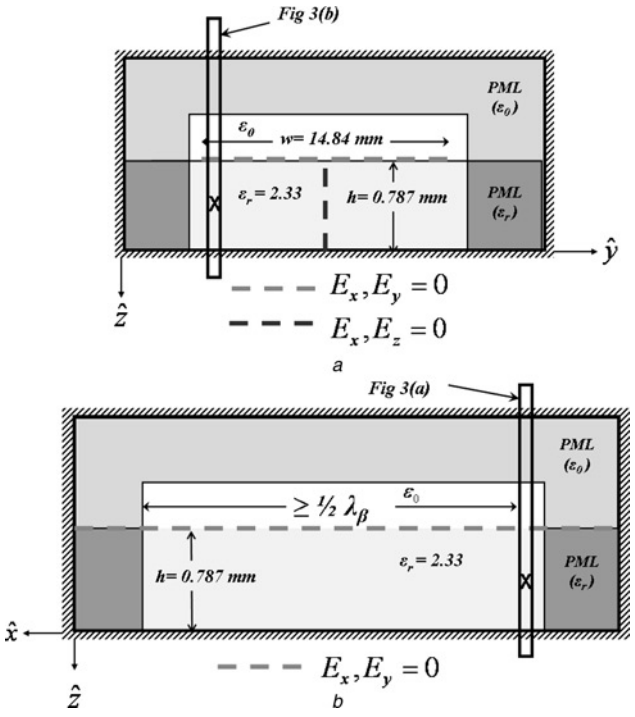


**Fig. 3** *2-D depiction of the 3-D computational space used to model the FW antenna*

*a* $\hat{y}$–$\hat{z}$ slice of the FW antenna extending into the UPML (not to scale); single source cell is marked by an *X*; $\hat{x}$–$\hat{z}$ slice of Fig. 3*b* is outlined
*b* $\hat{x}$–$\hat{z}$ slice of the FW antenna extending into the UPML (not to scale); $\hat{y}$–$\hat{z}$ slice of Fig. 3*a* is outlined
The co-ordinate system is consistent with Fig. 1*b*

### 2.3 Transverse resonance approximation

For comparison, a transverse resonance approximation was created following the work of Oliner and Lee [6, 23] which they confirmed with a steepest descent contour analysis. Fig. 4 shows a transmission line model that is applicable to the cross-section of the Menzel, FW and HW antennas. Each structure can be modelled as a dielectric-filled parallel plate waveguide of admittance $Y_{0\varepsilon}$ terminated at one end by a short circuit and the other end by admittance $Y_t$. The *E* null generated in the $\mathrm{EH}_1$ mode by a vertical wall or transverse slots is represented by a short circuit. $Y_t$ is an approximation of the admittance of an open edge of microstrip developed by Chang and Kuester [24, 25] using the Wiener–Hopf technique to analyse a TEM wave that is completely reflected.

The transverse resonance relation

$$\Gamma_{left}(y) \cdot \Gamma_{right}(y) = 1 \tag{3}$$

must hold for all points in the transverse $\hat{y}$-direction.

The reflection coefficient $\Gamma$ due to the admittance of the end of the microstrip $Y_t$ is unity with a phase shift $\chi$, as defined in [24, 25]. Referring to Fig. 4, at a point $y = y_a$ just to the right of $Y_t$

$$\Gamma_{left}(y_a) = \mathrm{e}^{j\chi} \tag{4}$$

$$\Gamma_{right}(y_a) = -\mathrm{e}^{-j2k\frac{w}{2}} \tag{5}$$

where $k = \beta - j\alpha$ is the complex wavenumber in the substrate and $w$ is the width of the structure. Equation (3) becomes

$$-e^{j(\chi - kw)} = 1$$
$$\chi - kw = \pm n\pi \quad n = 1, 3, 5, \ldots \tag{6}$$

$n = 1$ for the $\mathrm{EH}_1$ mode.

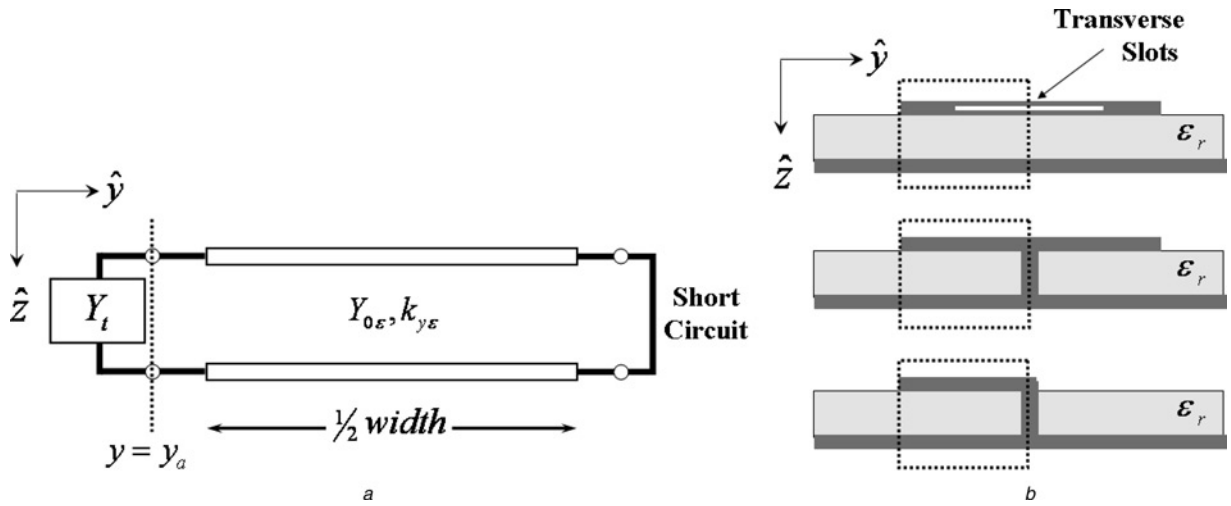


**Fig. 4** *Circuit model used with the transverse resonance approximation*

*a* Transmission line circuit that approximates the dotted cross-section of each of the three structures in (*b*) operating in mode $EH_1$
*b* Cross-sections of Menzel (top), FW (centre) and HW (bottom)

Fig. 5 shows that the transverse resonance approximation is in agreement to within 1% of the FDTD-derived $\beta$ data over the entire leaky band.

## 3 Results

### 3.1 Similarities/differences between HW, FW, Menzel

Generally our simulated and measured results showed the HW antenna to have advantages over the FW antenna and Menzel antenna. At most leaky band frequencies, the Menzel configuration used here had noticeably larger cross-polarisation (e.g. 10 dB at 6.2 GHz decreasing to 2 dB at 7.7 GHz) in the far-field as typified by the measurements in Fig. 6*a*. This is due in part to radiation by the nonresonant slots used to suppress the fundamental mode in the Menzel configuration. The cross-polarisation energy from the Menzel slots leads to decreased copolarisation gain measurements, as indicated in Fig. 6*b*. The copolarisation decrease of the Menzel configuration is typically of the order of 3 dB, although Fig. 6*b* shows an even greater reduction at 7.2 GHz. Further, the FDTD analysis shows that the slots in the Menzel design are not as effective in keeping the fundamental mode suppressed as is the longitudinal wall in the FW and HW antennas.

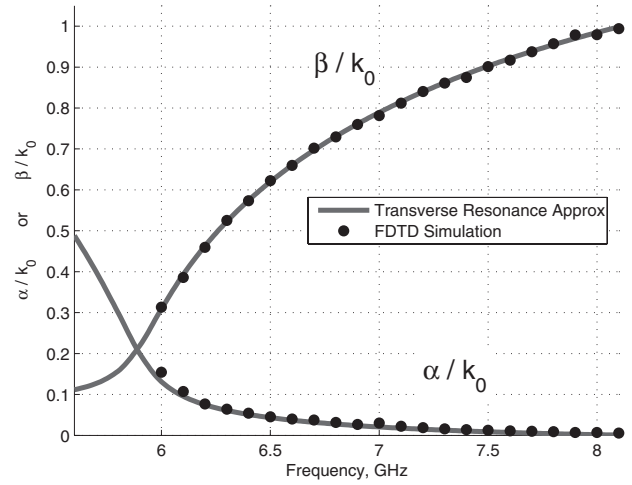


**Fig. 5** *FDTD simulation of the HW is in agreement with the transverse resonance approximation*

The copolarisation measurements show that the HW antenna, in which the wall was fabricated with vias spaced less than a tenth of a wavelength apart, has a slightly different mainbeam location and an increased backlobe. This difference is due to an uncertainty as to the effective width of the antenna since the vias are of finite diameter

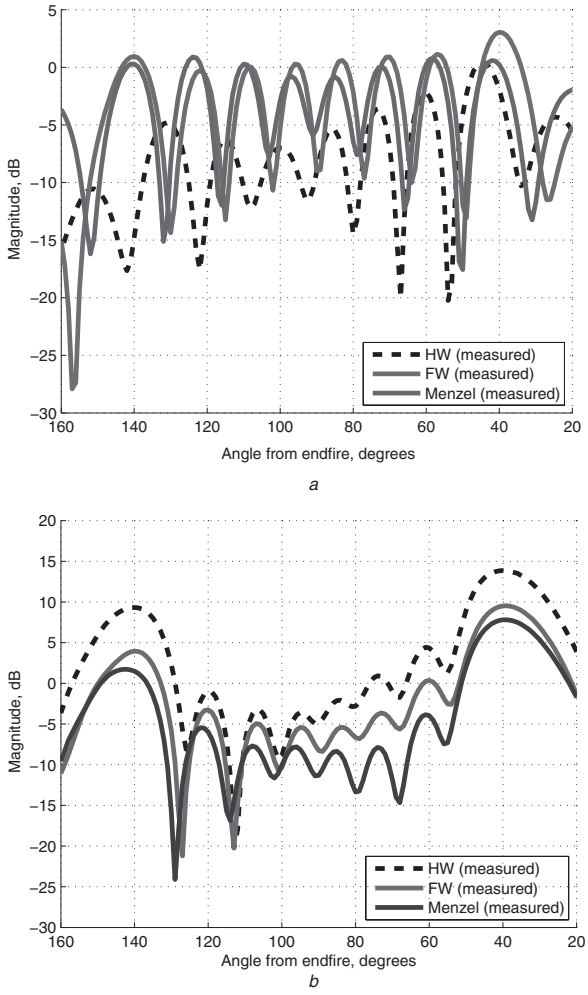


**Fig. 6** *Measured far-field patterns of the HW, FW, and Menzel antennas at 7.2 GHz*

*a* Cross-polarised
*b* Co-polarised

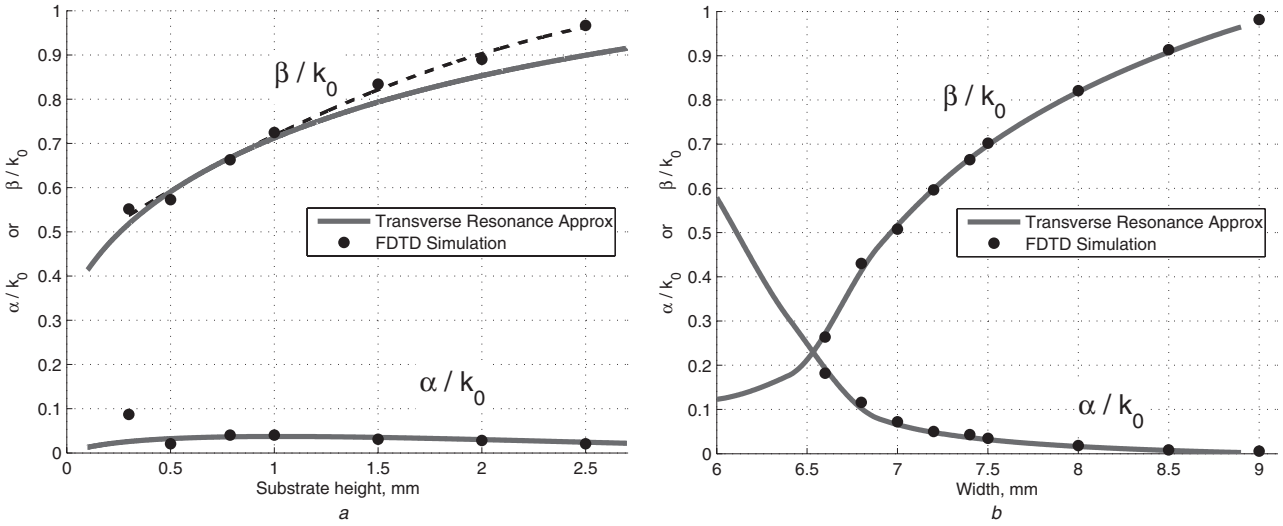


**Fig. 7** *Simulated effects at 6.7 GHz of varying the (a) height and (b) conductor width with the other parameters unchanged*

Dashed line in (*a*) is a quadratic least square of the FDTD data points; Parameters of the HW antenna are $h = 0.787$ mm, $\varepsilon_r = 2.33$ and $w = 7.5$ mm

and merely approximate a solid wall. The effective width significantly affects $\alpha$ and $\beta$ [26]. Slightly reducing the width of the HW by 0.15 mm matched the $\alpha$ and $\beta$ of the FW and Menzel antennas seen in Fig. 6*b*.

Our simulated results confirmed that $\alpha$ and $\beta$ of the FW and HW antennas were the same, as anticipated by image theory. Further, the FW antenna induced fields in the passive side that degraded the 180° phase difference across the width of the antenna [26]. This resulted in decreased radiation efficiency (i.e. reduced measured gain) for the FW antenna relative to a HW antenna with the same $\beta$, as evidenced in Fig. 6*b*.

### 3.2 Limitations of the transverse resonance approximation

The transverse resonance model was useful to get a quick approximation; however, a new model would be needed for geometries other than those in Fig. 1. In addition, the $Y_t$ approximation is not valid when the microstrip is curved or tapered.

Kuester *et al*. [25] state applicability to only *electrically-thin* substrates in which

$$h \ll \frac{1}{\omega\sqrt{\varepsilon\mu}} \tag{7}$$

For a substrate thickness $h = 0.787$ mm, (7) requires frequencies $\ll$40 GHz, which is five times higher than the highest frequency of this leaky band. Fig. 7*a* shows that FDTD and transverse resonance begin to disagree as the height of the substrate increases past the *electrically-thin* criteria of (7), near $h = 1.1$ mm at 6.7 GHz.

### 3.3 Modifying dimensions to meet bandwidth specifications

The leaky bandwidth is defined by $\alpha = \beta$ at the lower end and $\beta = k_0$ at the upper end [1]. Bandwidth around a desired centre frequency $f_c$ can be achieved by scaling the width of the conducting strip, the height (or thickness) of the substrate and/or the permittivity of the substrate. The bandwidth can be increased, to a limited extent, by the selection of the substrate material. As a fraction of the centre frequency, the percent bandwidth will be unaffected by altering the height and width, although $f_c$ can be readily shifted. The choice of substrate material and thickness is usually dictated by cost or availability of material, therefore, the width is typically the parameter to manipulate.

Fig. 7*a* illustrates the relationship between the height, or thickness, of the substrate and the propagation constant. Like permittivity, the height of the substrate is usually dictated by the material available. All antennas simulated and fabricated for this work used material that was 0.787 mm thick. As mentioned in the previous section, the transverse resonance solution includes an approximation that limits its applicability to *electrically-thin* substrates. The difference in $\beta$ between FDTD and transverse resonance becomes noticeable for heights greater than approximately $0.0375\lambda$, which is 1.1 mm at 6.7 GHz.

Fig. 7*b* shows that the propagation constant is very sensitive to the width of the conductor strip. As little as 0.1 mm difference in width will cause as much as 10% change in $\beta$. This sensitivity to width requires adequate fabrication precision.

### 3.4 Effect of curvature on $\alpha$ and $\beta$

Shown in Fig. 8 is a curved HW antenna with its wall along the inside edge. Simulations were done at radii of 3.36, 4.23, 5.32 and 9.3 cm. 180° was simulated when possible. Only

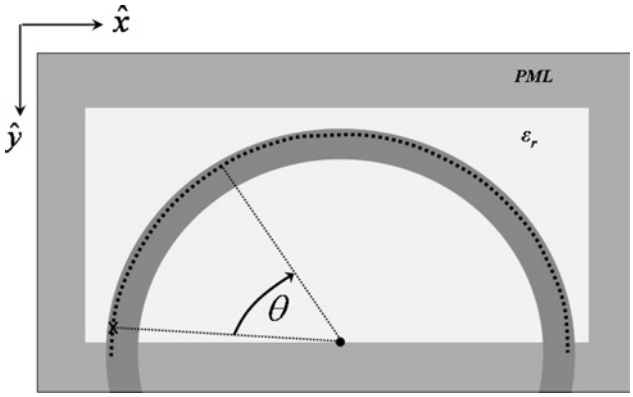


**Fig. 8** *180° curved HW antenna computational domain with the wall on the inside of the curve*

Source cell marked by the *X* in the lower left of the figure; guided travelling wave extracted from the cells marked by the dotted line along the open edge using angular position $\theta$ with respect to the source cell

**Table 1: Summary of curvature trials**

| | 180° | 180° | 180° | 90° | Straight |
|---|---|---|---|---|---|
| Radius (cm) | 3.36 | 4.23 | 5.32 | 9.3 | ∞ |
| Arc length (cm) | 10.6 | 13.3 | 16.7 | 14.6 | N/A |
| Largest $\lambda\beta$ possible (cm) | 21.2 | 26.6 | 33.4 | 29.2 | N/A |
| Lowest $f$ possible (GHz) | 6.2 | 6.1 | 6.0 | 6.1 | N/A |
| Approx. bandwidth (GHz) | 2.8 | 2.7 | 2.6 | 2.5 | 2.3 |

Bandwidth is the frequency difference between $\beta = \alpha$ and $\beta = k_o$

90° was simulated for the 9.3 cm radius model due to availability of computing resources.

All *curved* HW antenna models used a grid discretisation of $[dx : dy : dz] = [0.2361 : 0.2361 : 0.1574]$ mm, which is $[1.5 : 1.5 : 1]$. The size of the FDTD computational domain for the antenna modelled with a radius of 3.36 cm was [Nx, Ny, Nz]= [337, 184, 5], resulting in 310 040 cells, not including the PML. Similarly, the 4.23 cm radius used 411 450 cells, the 5.32 cm radius used 620 655 cells and the 9.3 cm radius used 907 380 cells. The size of the computational domain of all curved simulations necessitated only single precision, due to the 1 GB memory limitation. Like the straight antenna models, the length of the curved antennas needs to be longer than one-half $\lambda_\beta$ to extract the wavenumber. No subgridding of the curved edges was necessary since the resolution for all FDTD trials of curved antennas was over 100 cells per wavelength in the dielectric.

The curvature trials are summarised in Table 1. Fig. 9 shows that curvature increases bandwidth somewhat by flattening $\beta$, predominantly for the lower frequencies, while keeping $\alpha$ relatively unaffected. As the radius of curvature decreases, the bandwidth increases.

Curvature with the wall on the outside hampers the ability of the antenna to set up only the $EH_1$ mode. As seen in Fig. 10, a 180° arc of radius 4.23 cm produces destructive interference indicating the presence of one or more other modes.

### 3.5 Effect of multiple elements on $\alpha$ and $\beta$

The main beam of a travelling wave antenna is frequency-steerable in the longitudinal direction from near endfire to near broadside. A linear array of HW elements is, therefore, able to scan in two dimensions. A first step to developing such an array is to determine the effect of spacing between neighbouring elements. Two elements were simulated next to each other at 7.2 GHz. The results were nearly identical regardless of whether the second element was excited or not. The impact on the propagation

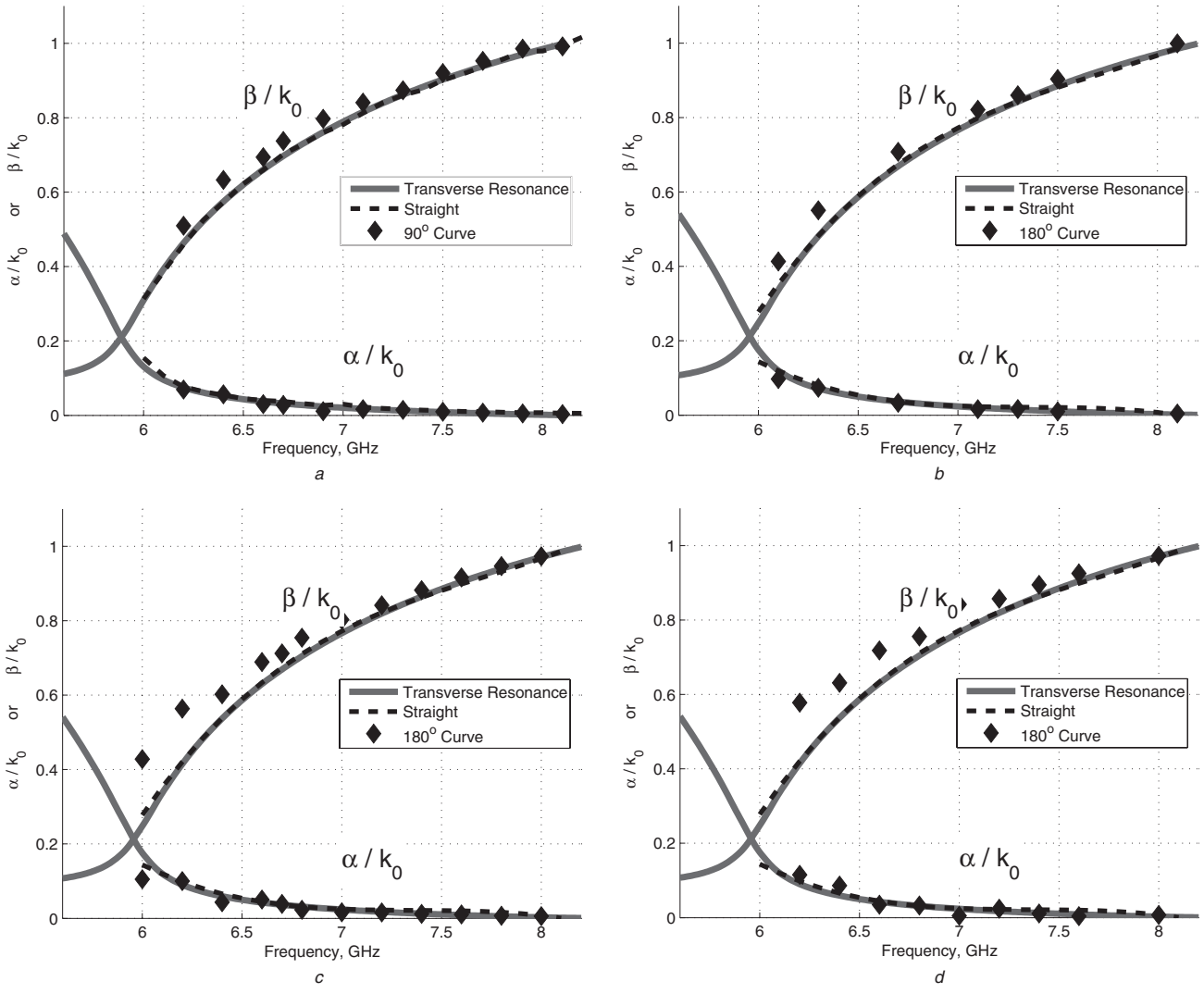


**Fig. 9** *FDTD simulated data for a curved HW antenna with a radius of (a) 93 mm (b) 53 mm (c) 42 mm (d) 34 mm*
For comparison, the single precision *curved* data is plotted alongside the single precision *straight* data

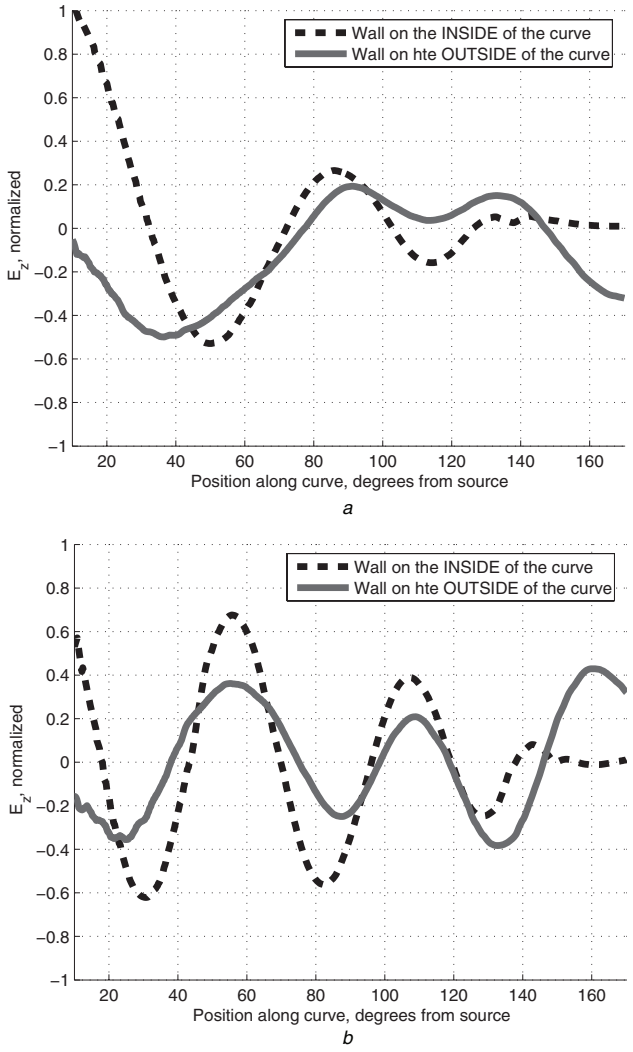


**Fig. 10** *FDTD simulations of a curved HW antenna with the wall on the outside produces field distributions, suggesting the presence of multiple modes*

*a* 6.4 GHz
*b* 7.4 GHz

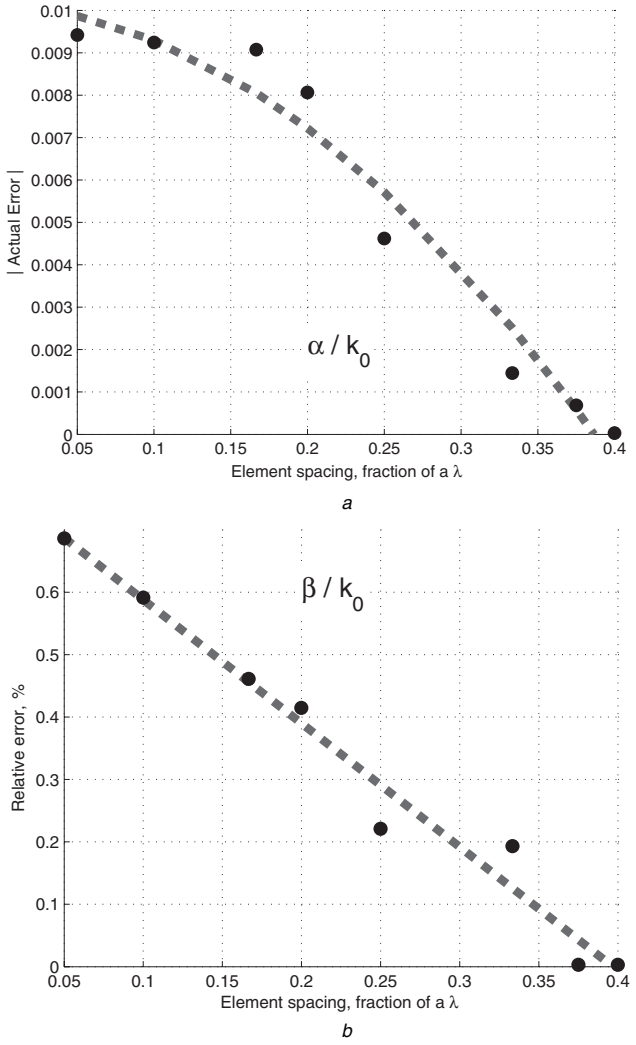


**Fig. 11** *Impact of neighboring element on the HW antenna's propagation constant*

*a* Actual error of $|\alpha|$ (dashed line is quadratic least square)
*b* Relative error of $\beta$ (dashed line is linear least square) from placing another element a fraction of a wavelength from the open end of the antenna in FDTD simulations
For both figures, the error is with respect to the guided wavenumber of a single element

constant by a neighbouring element is shown in Fig. 11. There is minimal interaction between elements if they are separated by at least 0.25 $\lambda$ and virtually no interaction if the spacing is over 0.4 $\lambda$.

## 4 Conclusions

The half-width (HW) leaky wave antenna was shown to be an improvement over the previously reported full-width (FW) antenna as well as the original Menzel antenna in the following ways:

1. The vertical wall used in the HW and FW antennas was found to be better at suppressing the fundamental mode than the slots in the Menzel antenna.
2. Since the mode purity in the HW and FW antennas is assured by the vertical wall, the feeding of these two antennas is simplified; for example, just a simple matched microstrip transmission line is required for the HW antenna or a 180° hybrid and matched transmission line for the FW antenna.
3. The slots in the Menzel configuration were found, in the pattern measurements and in the FDTD modelling, to contribute noticeably to cross-polarisation. The cross-polarisation of the HW pattern was typically found to be 3–6 dB lower than that of the Menzel design.
4. With the vertical wall used here, image theory suggests that one-half of the FW antenna may be discarded. In fact, it was found in the FDTD computations and in the pattern measurements, that the presence of the passive side reduced the radiation efficiency, since the unintentional excitation of the passive side degraded the 180° phase difference across the width of the FW antenna.
5. Our FDTD modelling indicates that there was no effect observed on the propagation constant of parallel HW elements if the spacing distance was greater than 0.4 $\lambda$. This relation simplifies design in an array environment
6. The (*H*-plane) curved HW was investigated and found to retain mode purity. It is unlikely that a FW (with a vertical wall) or Menzel design could achieve this. As a function of (*H*-plane) HW curvature, no significant impact to $\alpha$ was noticed compared to the straight case. However, the $\beta$ plot showed significant flattening, particularly at lower frequencies. Flattening $\beta$ without affecting $\alpha$ results in a bandwidth increase.

The primary tool in this investigation was three-dimensional FDTD modelling, the results of which agreed with the transverse resonance method. Experimental

measurements were confined to far-field patterns because previous work [19] indicated that the FDTD results for the complex propagation constant were more accurate than could reasonably be expected from experimental probe measurements.

A method was introduced in Section 2.1 to extract the complex propagation constant from FDTD data. It is believed that this method has not been previously developed. In addition, several means were found to decrease the number of FDTD cells required to accurately model the antennas investigated here. This allowed elaborate simulations using only a standard desktop PC with 1 GB of memory. Thus, high-performance computing resources, which are typically required for such simulations, were not needed and not used.

## 5 Acknowledgments

The authors would like to acknowledge the technical support by Dr. D. Janning and the measurement support of J. Radcliffe, both of the Air Force Research Laboratory (AFRL) Radiation and Scattering Compact Antenna Laboratory (RASCAL) facility. The foundation FDTD code was graciously furnished by Dr. S Hagness and K Willis of the University of Wisconsin Computational Electromagnetics Laboratory. Although their code was extensively rewritten and modified for our purposes, it provided an excellent starting point for our work. The views expressed in this article are those of the authors and do not reflect the official policy or position of the United States Air Force, Department of Defense, or the United States Government.

## 6 References

1 Oliner, A.A.: 'Leakage from higher modes on microstrip line with applications to antennas', *Radio Sci.*, 1987, **22**, (6), pp. 907–912
2 Bagby, J.S., Nyquist, D.P., Lee, C.-H., and Yuan, Y.: 'Identification of propagation regimes on integrated microstrip transmission lines', *IEEE Trans. Microw. Theory Tech.*, 1993, **41**, (11), pp. 1887–1894
3 Ermert, H.: 'Guided modes and radiation characteristics of covered microstrip lines', *Arch. Elektron. Ubertrag. technik*, 1976, **30**, (2), pp. 65–70
4 Ermert, H.: 'Guiding and radiation characteristics of planar waveguides', *Microw. Opt. Acoust.*, 1979, **3**, (2), pp. 59–62
5 Menzel, W.: 'A new travelling-wave antenna in microstrip', *Arch. Elektroni. Ubertrag. technik (AEU)*, 1979, **33**, (4), pp. 137–140
6 Oliner, A.A., and Lee, K.S.: 'The nature of the leakage from higher modes on microstrip line'. IEEE MTT-S Int. Microwave Symp. Digest, 1986, pp. 57–60
7 Oliner, A.A., and Lee, K.S.: 'Microstrip leaky wave strip antennas'. Proc. Antennas and Propagation Soc. Int. Symp, June 1986, vol. 24, pp. 443–446
8 Chen, S.-D., and Tzuang, C.-K.C.: 'Characteristic impedance and propagation of the first higher order microstrip mode in frequency and time domain', *IEEE Trans. Microw. Theory Tech.*, 2002, **50**, (5), pp. 1370–1379
9 Lin, Y.-D., and Sheen, J.-W.: 'Mode distinction and radiation efficiency analysis of planar leaky-wave line source', *IEEE Trans. Theory Tech.*, 1997, **45**, (10), pp. 1540–1543
10 Mesa, F., Jackson, D.R., and Freire, M.J.: 'Evolution of leaky modes on printed-circuit lines', *IEEE Trans. Microw. Theory Tech.*, 2002, **50**, (1), pp. 94–104
11 Jackson, D.R., and Oliner, A.A.: 'A leaky-wave analysis of the high-gain printed antenna configuration', *IEEE Trans. Antennas Propag.*, 1988, **36**, (7), pp. 905–910
12 Janning, D., and Thiele, G.A.: 'Conformal microstrip leaky wave antenna'. U.S. Patent Application, 9 February 2005
13 Hong, W., Chen, T.-L., Chang, C.-Y., Sheen, J.-W., and Lin, Y.-D.: 'Broadband tapered microstrip leaky-wave antenna.', *IEEE Trans. Antennas Propag.*, 2003, **51**, (8), pp. 1922–1928
14 Hu, C.-N., Tzuang, C.-K., and Chen, S.-D.: 'A novel design for the microstrip leaky-mode antenna array with high efficiency', *IEEE Trans. Microw. Theory Tech.*, 2000, **41**, (11), pp. 247–250, 21–25
15 Nalbian, V., and Dee, C.S.: 'Bandwidth enhansement of microstrip antenna with leaky-wave excitation'. 1999 IEEE Antennas and Propagation Soc. Int. Symp., 1999, vol. 2, pp. 1224–1227, 11–16
16 Nalbian, V., and Dee, C.S.: 'Tapered leaky-wave ultrawide-band microstrip antenna'. 1999 IEEE Antennas and Propagation Soc. Int. Symp., July 1999, vol. 2, pp. 1236–1239, 11–16
17 Tzuang, C.-K.C.: 'Leaky-mode perspective on printed antenna', *Proc. Nat. Sci. Counc., Rep. China*, 1999, **23**, (4), pp. 544–548
18 Walter, C.H.: 'Traveling wave antennas' (McGraw-Hill, New York, NY, 1965)
19 Radcliffe, J.S., Thiele, G.A., and Zelinski, G.M.: 'A microstrip leaky wave antenna and its properties'. 26th Antenna Measurement Techniques Association (AMTA) Symp, October 2004
20 Lee, K.F., Guo, Y.X., Hawkins, J.A., Chair, R., and Luk, K.M.: 'Theory and experiment on microstrip patch antennas with shorting walls', *IEE Proc., Microw. Antennas Propag.*, 2000, **147**, (6), pp. 521–525
21 Taflove, A., and Hagness, S.: 'Computational electrodynamics: The finite difference time-domain method' (Artech House, Boston, MA, 2000, 2nd edn.)
22 Sheen, D.M.: 'Numerical modeling of microstrip circuits and antennas'. PhD dissertation, Massachusetts Institute of Technology, Cambridge, MA, U.S.A, 1991
23 Lee, K.S.: 'Microstrip line leaky wave antennas'. PhD dissertation, Polytechnic Institute of New York, NY, USA, 1986
24 Chang, D.C., and Kuester, E.F.: 'Total and partial reflection from the end of a parallel-plate waveguide with an extended dielectric slab', *Radio Sci.*, 1981, **16**, (1), pp. 1–13
25 Kuester, E.F., Johnk, R.T., and Chang, D.C.: 'The thin-substiate approximation for reflection from the end of a slab-loaded parallel-plate waveguide with applications to microstrip patch antennas', *IEEE Trans. Antennas Propag*, 1982, **30**, (5), pp. 910–917
26 Zelinski, G.M.: 'Finite difference time domain analysis of a leaky traveling wave microstrip antenna'. Master's Thesis, Air Force Institute of Technology, Wright-Patterson AFB, OH, USA, 2005